Acta Pharmaceutica Sinica B 2020;10(9):1730–1740

Chinese Pharmaceutical Association
Institute of Materia Medica, Chinese Academy of Medical Sciences

Acta Pharmaceutica Sinica B

www.elsevier.com/locate/apsb
www.sciencedirect.com

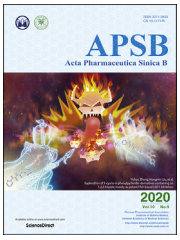

ORIGINAL ARTICLE

# Remote loading paclitaxel–doxorubicin prodrug into liposomes for cancer combination therapy

**Jiang Yu[a,†], Yingli Wang[a,†], Shuang Zhou[a], Jinbo Li[a], Jiamei Wang[a], Dongxu Chi[b], Xue Wang[b], Guimei Lin[c], Zhonggui He[a], Yongjun Wang[a,*]**

[a]*Wuya College of Innovation, Shenyang Pharmaceutical University, Shenyang 110016, China*
[b]*Department of Pharmaceutics, Shenyang Pharmaceutical University, Shenyang 110016, China*
[c]*School of Pharmaceutical Science, Shandong University, Jinan 250012, China*

Received 15 February 2020; received in revised form 17 March 2020; accepted 18 March 2020

**KEY WORDS**

Combination therapy;
Nanoparticles;
Paclitaxel–doxorubicin prodrug;
Remote loading liposomes;
Prodrug;
Safety

**Abstract** The combination of paclitaxel (PTX) and doxorubicin (DOX) has been widely used in the clinic. However, it remains unsatisfied due to the generation of severe toxicity. Previously, we have successfully synthesized a prodrug PTX-*S*-DOX (PSD). The prodrug displayed comparable *in vitro* cytotoxicity compared with the mixture of free PTX and DOX. Thus, we speculated that it could be promising to improve the anti-cancer effect and reduce adverse effects by improving the pharmacokinetics behavior of PSD and enhancing tumor accumulation. Due to the fact that copper ions ($Cu^{2+}$) could coordinate with the anthracene nucleus of DOX, we speculate that the prodrug PSD could be actively loaded into liposomes by $Cu^{2+}$ gradient. Hence, we designed a remote loading liposomal formulation of PSD (PSD LPs) for combination chemotherapy. The prepared PSD LPs displayed extended blood circulation, improved tumor accumulation, and more significant anti-tumor efficacy compared with PSD NPs.

*Abbreviations:* ALT, alanine transaminase; AST, aspartate transaminase; AUC, area under the curve; BUN, blood urea nitrogen; CHO, cholesterol; $CO_2$, carbon dioxide; CR, creatinine; $Cu^{2+}$, copper ions; DL, drug loading; DLS, dynamic light scattering; DMSO, dimethyl sulfoxide; DNA, deoxyribonucleic acid; DOX, doxorubicin; DSPE-PEG2000, 2-distearoyl-snglycero-3-phosphoethanolamine-*N*-[methyl(polyethylene glycol)-2000; DTT, D,L-dithiothreitol; EDTA, ethylene diamine tetraacetic acid; EE, encapsulation efficacy; FBS, fetal bovine serum; GSH, glutathione; H&E, hematoxylin and eosin; $H_2O_2$, hydrogen peroxide; HEPES, 4-(2-hydroxyethyl)-1-piperazineethanesulfonic acid; HPLC, high-performance liquid chromatography; HSPC, hydrogenated soybean phospholipids; $IC_{50}$, half maximal inhibitory concentration; IVIS, *in vivo* imaging system; MLVs, multilamellar vesicles; MRT, mean residence time; MTD, maximum tolerated dose; MTT, 3-(4,5-dimethylthiazol-2-yl)-2,5-diphenyltetrazolium bromide; PBS, phosphate buffer saline; PDI, polydispersity index; PSD LPs, PTX-*S*-DOX liposomes; PSD NPs, PTX-*S*-DOX self-assembled nanoparticles; PSD, PTX-*S*-DOX; PTX, paclitaxel; ROS, reactive oxygen species; SD, standard deviation; TEM, transmission electron microscopy; UV, ultraviolet.

*Corresponding author. Tel./fax: +86 24 23986325.
E-mail address: wangyongjun@syphu.edu.cn (Yongjun Wang).
†These authors made equal contributions to this work.

Peer review under responsibility of Chinese Pharmaceutical Association and Institute of Materia Medica, Chinese Academy of Medical Sciences.

https://doi.org/10.1016/j.apsb.2020.04.011

2211-3835 © 2020 Chinese Pharmaceutical Association and Institute of Materia Medica, Chinese Academy of Medical Sciences. Production and hosting by Elsevier B.V. This is an open access article under the CC BY-NC-ND license (http://creativecommons.org/licenses/by-nc-nd/4.0/).

Furthermore, PSD LPs exhibited reduced cardiotoxicity and kidney damage compared with the physical mixture of Taxol and Doxil, indicating better safety. Therefore, this novel nano-platform provides a strategy to deliver doxorubicin with other poorly soluble antineoplastic drugs for combination therapy with high efficacy and low toxicity.

© 2020 Chinese Pharmaceutical Association and Institute of Materia Medica, Chinese Academy of Medical Sciences. Production and hosting by Elsevier B.V. This is an open access article under the CC BY-NC-ND license (http://creativecommons.org/licenses/by-nc-nd/4.0/).

## 1. Introduction

In the past decades, due to the low therapeutic efficacy and generation of drug resistance caused by a single drug or therapy strategy, combination chemotherapy has been developed to improve the anticancer efficacy and reduce side effects by achieving synergistic therapeutic efficacy[1−3]. However, conventional cocktail combination chemotherapeutics usually deviate from the prediction on account of rapid blood clearance and diverse pharmacokinetics among different drugs[1,4,5]. Paclitaxel (PTX) and doxorubicin (DOX) are both common chemotherapeutic agents used in the clinic[6,7]. PTX, as a cell-cycle specific drug, induced the apoptosis of tumor cells by blocking cell cycle progression in the late G2-M phases[8,9]. On the contrary, DOX was a cell-cycle non-specific drug. The proposed mechanisms of action for DOX included inhibition of topoisomerase II, intercalation into deoxyribonucleic acid (DNA) and generation of reactive oxygen species[10]. The combination of PTX and DOX has been widely used for treating multiple types of cancer[11]. The combination chemotherapy of different anti-tumor mechanism drugs was beneficial to reduce drug resistance and improve therapeutic efficacy[12,13]. However, the combination of free PTX and DOX remained unsatisfied due to the generation of serious toxicities to normal tissue, such as cardiotoxicity and neurotoxicity[11,14,15]. Therefore, it is necessary to precisely deliver two drugs using a highly effective and low-toxicity formulation.

Previously, our group has successfully synthesized a heterodimeric prodrug paclitaxel-*S*-doxorubicin (PTX-*S*-DOX, PSD, Supporting Information Fig. S1) for combination chemotherapy[16]. Compared with the mixture of free PTX and DOX, the PSD NPs displayed comparable *in vitro* cytotoxicity and improved antitumor efficacy *in vivo*. Nevertheless, in spite of enhancing half-time compared with free drugs, prodrug self-assembled nanoparticles still exhibited rapid clearance after intravenous administration, which could be attributed to the instability of nanoparticles in the blood. Thus, we speculate that it is promising to improve the anti-cancer effect by improving the pharmacokinetics behavior of PSD and enhancing tumor accumulation.

With the rapid development of nanotechnology, liposomes have emerged as an efficient nano-carrier among numerous nanoplatforms[17,18]. Liposomes have the advantages of enhancing blood circulation time, coordinating pharmacokinetics of drugs, and reducing the toxicity to normal tissues[3,19]. However, generally, the hydrophobic drug PTX could not be loaded into liposomes by remote loading method. On the contrary, it is usually incorporated into the lipid layer of liposomes, which are with poor stability and limited drug loading capacity[20,21]. Thus, this limits the combination of PTX and DOX utilizing a remote loading liposomal formulation. It is reported that copper ions ($Cu^{2+}$) could bind with the anthracene nucleus of DOX to form a stable complex (Cu−DOX), and DOX could be loaded into liposomes using a $Cu^{2+}$ gradient[22−24]. Furthermore, there has been reported that the formation of Cu−DOX complexation could induce the death of tumor cells, which is mediated by the generation of reactive oxygen species (ROS), the damage of DNA strand, and lipid peroxidation[25−27]. Due to the fact that the structure of anthracene nucleus for DOX was reserved in PSD, we speculate that the prodrug PSD also has the potential to be encapsulated into the liposomes utilizing a $Cu^{2+}$ gradient.

Based on these considerations, we designed a remote loading liposomal formulation for combination chemotherapy, which utilizes a $Cu^{2+}$ gradient to encapsulate the prodrug PSD into the intraliposomal aqueous phase of liposomes (Fig. 1A). The prepared PSD liposomes (PSD LPs) exhibited prolonged blood circulation time, higher tumor accumulation and improved *in vivo* anti-cancer efficacy in comparison with PSD NPs, which were consistent with our hypotheses. In conclusion, this approach provides a novel strategy to deliver doxorubicin with hydrophobic drugs for combination chemotherapy utilizing a remote loading liposomal formulation.

## 2. Materials and methods

### 2.1. Materials and reagent

Paclitaxel was purchased from NanJing Jingzhu Bio-technology Co., Ltd. (Nanjing, China). Doxorubicin hydrochloride (DOX·HCl) and DiR were obtained from Meilun Biotech (Dalian, China). DTT and $H_2O_2$ were purchased from Aladdin (Shanghai, China). Hydrogenated soybean phospholipids (HSPC), cholesterol (CHO, for injection) and 2-distearoyl-*sn*-glycerol-3-phosphoethanolamine-*N*-methyl (polyethylene glycol)-2000 (DSPE-PEG2000) were purchased from Shanghai Advanced Vehicle Technology Pharmaceutical Ltd., (Shanghai, China). Sepharose CL-4B gel was bought from Beijing Solarbio Corporation (Beijing, China). Roswell Park Memorial Institute (RPMI-1640), 3-(4,5-dimethylthiazol-2-yl)-2,5-diphenyltetrazolium bromide (MTT) and trypsin were all purchased from Gibco (Beijing, China). 96-well plates were supplied by NEST Biotechnology (Wuxi, China). Fetal bovine serum (FBS) was purchased from Hyclone (Beijing, China). Dimethyl sulfoxide (DMSO) was acquired from Kemeng (Tianjin, China). All other reagents and solvents used in this work were of analytical grade or HPLC grade.

### 2.2. Synthesis of PSD prodrug

The redox dual-responsive prodrug PSD was synthesized by conjugating PTX with DOX using a thioether bond as linkage as described previously[16].

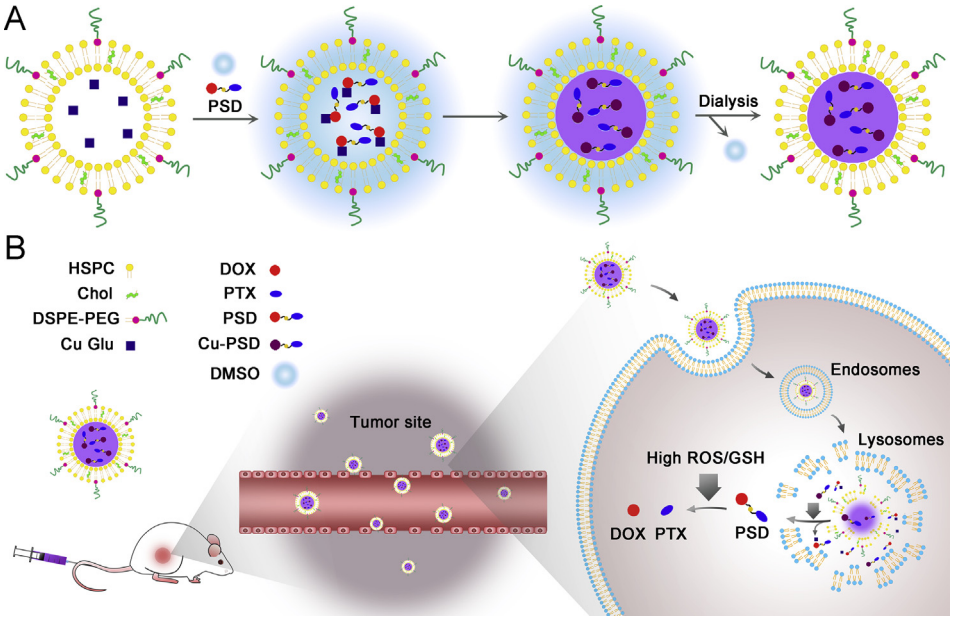


**Figure 1** (A) The schematic diagram for active loading of PTX-*S*-DOX (PSD) *via* a copper ion gradient. (B) Schematic representation of PSD LPs for cancer therapy.

### 2.3. *Preparation of PSD liposomes and nanoparticles*

The conventional thin-film hydration method was applied to prepare blank liposomes. Briefly, the lipids consisting of HSPC, cholesterol and DSPE-PEG2000 with a weight ratio of 85:5:10 were dissolved in chloroform, and the organic solvent was evaporated at 40 °C to form a thin-film. The thin-film was hydrated with 200 mmol/L copper gluconate at 65 °C for 1 h, pH adjusted to 7.4 with triethanolamine. The obtained multilamellar vesicles (MLVs) were then extruded 10 times through 400, 200, and 100 nm pore size polycarbonate membrane at 65 °C, sequentially. In order to remove un-encapsulated $Cu^{2+}$, the liposomes were passed through a Sepharose CL-4B gel column pre-equilibrated with SHE [300 mmol/L sucrose, 20 mmol/L 4-(2-hydroxyethyl)-1-piperazineethanesulfonic acid (HEPES), and 15 mmol/L ethylene diamine tetraacetic acid (EDTA), pH 7.4] buffer.

PSD was solubilized in DMSO at 10 mg/mL. The pre-dissolved drug was then slowly dropped to the copper-containing liposomes at 65 °C and incubated for 30 min, such that the final PSD to liposomal lipid ratio was 0.2 (*w*/*w*). The formulation was then immediately cooled for 15 min in an ice bath. So as to remove the residual EDTA and un-encapsulated drug, liposomes were exchanged into 300 mmol/L sucrose, 20 mmol/L HEPES (pH 7.4) buffer using a Sepharose CL-4B gel column. Furthermore, the residual DMSO was removed by dialysis. The final formulation was stored in a dark place at 4 °C.

Respectively, the preparation of PSD nanoparticles (PSD NPs) was the same as described previously[16].

### 2.4. *Preparation of DiR-labeled PSD liposomes and nanoparticles*

The preparation of DiR-labeled blank liposomes was used as a thin-film hydration method. The fluorescent dye DiR and lipids of the above formulation were dissolved in chloroform and evaporated at 40 °C to form a thin-film. The following steps were the same as described above.

The preparation of DiR-labeled PSD NPs was the same as described previously[16].

### 2.5. *Characterization of PSD LPs and PSD NPs*

Particle size, polydispersity index (PDI) and zeta potential of PSD LPs were determined utilizing a Zetasizer (Nano ZS, Malvern, UK) in triplicate.

The morphology of PSD LPs was observed through transmission electron microscopy (TEM, Hitachi, HT7700, Japan). About 10 μL of PSD LPs were dropped onto 200 mesh carbon-coated copper grid and retained for 30 s, and then stained by 0.2% phosphotungstic acid for 30 s.

The encapsulation efficiency of PSD was measured by gel filtration method with a Sepharose CL-4B gel column. Then 400 μL liposome samples were gently added on the Sepharose CL-4B gel column pre-equilibrated with 300 mmol/L sucrose, 20 mmol/L HEPES (pH 7.4) to remove the unencapsulated PSD. The concentration of drug was determined by HPLC (Hitachi) with acetonitrile and redistilled water (55:45, *v*/*v*) at a flow rate of 1.0 mL/min. The ultraviolet-visible detector was kept at 227 nm. The encapsulation efficiency (EE) and drug loading (DL) were calculated according to Eqs. (1) and (2):

$$\text{EE}\ (\%) = C_1/C_0 \times 100 \quad (1)$$

where $C_1$ represents the quantity of drug encapsulated in liposomes and $C_0$ is the total quantity of that drug.

$$\text{DL}\% = W_1/W_0 \times 100 \quad (2)$$

where $W_1$ is the quantity of drug encapsulated in liposomes, and $W_0$ is the quantity of the total liposomes.

### 2.6. Ultraviolet spectra

The ultraviolet (UV) absorbance spectra of Cu Glu in deionized water, free PSD in DMSO, $Cu^{2+}$−PSD complex in DMSO and PSD LPs in deionized water were obtained using a multimode microplate reader (Thermo Scientific, USA) within the wavelength range of 400−650 nm.

### 2.7. Physical stability

The PSD LPs (0.5 mg/mL) were stored at 4 °C for 1 month to evaluate the long-term stability of liposomes. The particle size, PDI and zeta potential were measured at given time intervals.

In addition, in a typical procedure, l mL PSD LPs (0.5 mg/mL) or PSD NPs (0.5 mg/mL) was incubated in 9 mL PBS (pH 7.4) containing 10% FBS (*v*/*v*) at 37 °C for 72 h. The size and PDI were measured at pre-determined intervals.

### 2.8. In vitro drug release

The *in vitro* drug release of PSD LPs was carried out by dialysis method at 37 °C under a shaking bed (100 rpm, CHA-S, Guohua Electric Appliance Co., Ltd., Changzhou, China). 400 μL of PSD LPs were added into a dialysis bag and suspended in 30 mL PBS (pH 7.4) containing 15% ethanol (*v*/*v*) and 10 mmol/L EDTA. The released behaviors for redox response were also accomplished as described above, except for the addition of 10 mmol/L $H_2O_2$ or DTT. At the predetermined time points, 200 μL of samples were taken for analysis and an equal volume of medium was replenished. The concentrations of PTX and DOX were determined by HPLC as mentioned previously.

### 2.9. Cell culture

4T1 cells (breast cancer cell line) were cultured in Gibco 1640 medium with 10% FBS, penicillin (30 μg/mL) and streptomycin (100 μg/mL). RM-1 cells (prostatic cancer cells line) were cultured in Gibco 1640 medium with 10% FBS, penicillin (30 μg/mL) and streptomycin (100 μg/mL), glucose (2.5 mg/mL). All cells were cultivated at 37 °C in a humidified atmosphere of 5% carbon dioxide ($CO_2$).

### 2.10. Cytotoxicity assay

The MTT assay was utilized to evaluate the anti-proliferative activity of blank Cu Glu LPs, PSD NPs and PSD LPs against 4T1 cells and RM-1 cells. Briefly, cells of a certain density (1000/well) were seeded in 96-well plates and cultivated for 24 h. Then the former culture medium was withdrawn. The cells were exposed to serial dilutions of blank Cu Glu LPs, PSD NPs and PSD LPs and further incubated for 12, 24, 48 or 72 h. The cells with fresh culture medium without drugs were utilized as control ($n = 3$ for each group). After incubation, 20 μL of MTT solution (5 mg/mL) was added and continuously incubated for another 4 h. After that, the solution was discarded carefully and 200 μL of DMSO in each well was added to dissolve the formed formazan crystals. Then, the absorbance of each well at 570 nm was determined with a microplate reader (Model 500, USA). The cell viability was calculated by Eq. (3):

$$\text{Cell viability } (\%) = A_{\text{sample}}/A_{\text{control}} \times 100 \quad (3)$$

which $A$ is the absorbance value. The $IC_{50}$ values were calculated using GraphPad Prism 6.0 (La Jolla, CA, USA).

### 2.11. Animals

All the animals were provided by the Laboratory Animal Center of Shenyang Pharmaceutical University (Shenyang, Liaoning, China, quality certificate number: 211002300041785, 1103221911000055). All the animal experiments were conducted according to the Guidelines for the Care and Use of Laboratory Animals, and received ethical approval from the Institutional Animal Ethical Care Committee (IAEC) of Shenyang Pharmaceutical University.

### 2.12. In vivo pharmacokinetic study

In order to investigate the pharmacokinetic profiles, male Sprague−Dawley rats weighing 200−230 g were divided into two groups randomly ($n = 3$ per group). Prior to the experiment, the rats were fasted for 12 h with free access to water. PSD NPs and PSD LPs were intravenously administrated to Sprague-Dawley rats at a dosage of 3 mg/kg PTX equivalent and 1.9 mg/kg DOX equivalent. At the predetermined time points (0.083, 0.25, 0.5, 1, 2, 4, 8, 12, 24 and 48 h), blood samples were collected and then centrifuged to obtain the plasma. The concentration of prodrug and free drug was monitored by UPLC−MS/MS (Waters Co., Ltd., Milford, MA, USA). The pharmacokinetic parameters were calculated using DAS 2.0 (Shanghai BioGuider Medicinal Technology Co., Ltd., Shanghai, China).

### 2.13. In vivo bio-distribution study

For the purpose of exploring *in vivo* bio-distribution of PSD NPs and PSD LPs, the female BALB/c mice (20−22 g) bearing 4T1 xenograft tumors were established. When the tumor volume reached around 200 $mm^3$, the mice were intravenously administrated with DiR-labeled PSD NPs and DiR-labeled PSD LPs (2 mg/kg DiR equivalent, $n = 6$ per group). The *in vivo* optical imaging of mice was investigated using a noninvasive optical *in vivo* imaging system (IVIS) spectrum small-animal imaging system with an excitation wavelength of 748 nm at the predetermined time points 1, 4, 8, 12, 24, and 48 h. At 24 or 48 h post-injection, three mice of every group were sacrificed and the major organs (heart, liver, spleen, lung, and kidney) and tumors were collected for *ex vivo* fluorescence imaging.

When the tumor volume reached around 200 $mm^3$, the PSD NPs and PSD LPs (10.6 mg/kg for PSD) were administrated intravenously. The mice were sacrificed at 6, 24 and 48 h post-injection and tumors were collected. The concentration of drugs was detected by a microplate reader (Model 500).

### 2.14. In vivo anticancer efficacy

The female BALB/c mice (20−22 g) bearing 4T1 xenograft tumors were established to evaluate *in vivo* anti-tumor effect. 4T1 cells ($5 \times 10^6$ cells in 200 μL) were injected subcutaneously in the right flank region of BALB/c mice. The tumors were permitted to grow to an average tumor volume of 100 $mm^3$ before initiation of administration. Then, the mice were randomly divided into 7 groups ($n = 5$). Animals in each group were administered every three days *via* a lateral tail vein for a total of four times with saline, blank Cu Glu LPs, Taxol, Doxil, Taxol + Doxil, PSD NPs and PSD LPs (6 mg/kg PTX equivalent, 3.8 mg/kg DOX equivalent), respectively. The tumor volume and body weight change were recorded every two days. All the mice were sacrificed on the

**Table 1** Characterization of PSD LPs.

| Formulation | Size (nm) | PDI | Zeta potential (mV) | EE (%) | DL (%) |
|---|---|---|---|---|---|
| Blank Cu Glu LPs | 112.4 ± 2.458 | 0.036 ± 0.049 | −21.1 ± 0.473 | – | – |
| PSD LPs | 128.5 ± 2.610 | 0.094 ± 0.003 | −21.3 ± 0.608 | 98.4 ± 1.6 | 16.4 ± 0.3 |

EE and DL refer to encapsulation efficiency and drug loading, respectively.
Data are mean ± S.D., $n = 3$.

eleventh day, and the blood of mice was collected for hepatic function and renal function marker measurements. The tumors and major organs (heart, liver, spleen, lung, and kidney) were excised, weighed, and fixed in 4% paraformaldehyde for staining with hematoxylin and eosin (H&E) to evaluate the pathological changes.

### 2.15. *Statistical analysis*

Data were calculated and treated as mean value ± standard deviation (S.D.). Statistical difference between different groups was analyzed with student's *t*-test and one-way analysis of variance, and $P$ values less than 0.05 ($P < 0.05$) were considered statistically significantly different.

## 3. Results and discussion

### 3.1. *Synthesis of PSD prodrug*

A redox-responsive prodrug PSD was successfully synthesized by conjugating PTX and DOX with a single thioether bond as linkage (Fig. S1).

### 3.2. *Preparation and characterization of PSD LPs*

Previously, we have successfully synthesized a prodrug PSD and the structure of anthracene nucleus for DOX was reserved. It has been reported that the anthracene nucleus of DOX could bind with $Cu^{2+}$ forming a steady insoluble complex (Cu−DOX), and DOX could be loaded into liposomes using a $Cu^{2+}$ gradient[22,24]. Thus, we speculate that the prodrug PSD also has the potential to be encapsulated into the liposomes utilizing a $Cu^{2+}$ gradient. Therefore, a novel remote loading liposomal formulation for the combination of PTX and DOX was prepared utilizing a metal ion gradient method.

Blank Cu Glu LPs were prepared by thin-film hydration method. PSD was dissolved in DMSO at a concentration of 10 mg/mL and was gently added to blank copper-containing liposomes incubating for 30 min at 65 °C. The characterization results of PSD LPs were shown in Table 1 and Fig. 2. The particle size, PDI and zeta potential of blank Cu Glu liposomes were 112.4 ± 2.458 nm, 0.036 ± 0.049 and −21.1 ± 0.473 mV, respectively. After drug loading, the particle size, PDI and zeta potential were changed to 128.5 ± 2.610 nm, 0.094 ± 0.003 and −21.3 ± 0.608 mV, correspondingly. Moreover, the PSD LPs exhibited a high encapsulation efficiency (98.4 ± 1.6%) and drug loading (16.4 ± 0.3%). Meanwhile, the drug remote loading process was time- and temperature-dependent. As shown in Fig. 2C, the encapsulation efficiency was gradually increased with the extension of incubating time until 30 min, for which almost all drugs have been entrapped into liposomes. However, when the incubation temperature reduced, the encapsulation efficiency decreased respectively, which could attribute to the reduced transmembrane rate of drugs (data not shown).

In order to confirm the formation of $Cu^{2+}$−PSD complex in the intraliposomal aqueous phase, the UV absorption spectra of $Cu^{2+}$, free PSD, $Cu^{2+}$−PSD and PSD LPs were investigated. As shown in Fig. 2D, the UV spectra of $Cu^{2+}$−PSD showed an obvious bathochromic shift and broadened absorption band

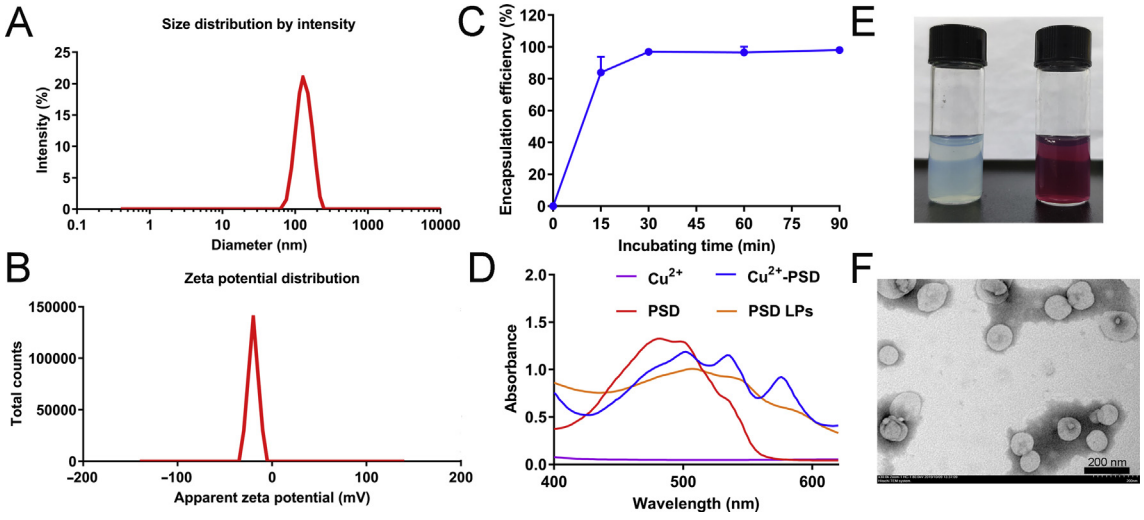


**Figure 2** (A) The particle size and (B) zeta potential of the prepared PSD LPs. (C) Encapsulation efficiency variation curve with incubation time (mean ± SD, $n = 3$). (D) The UV absorption spectra of $Cu^{2+}$, free PSD, $Cu^{2+}$−PSD and PSD LPs. (E) The photograph of blank Cu Glu LPs and PSD LPs. (F) TEM image of PSD LPs.

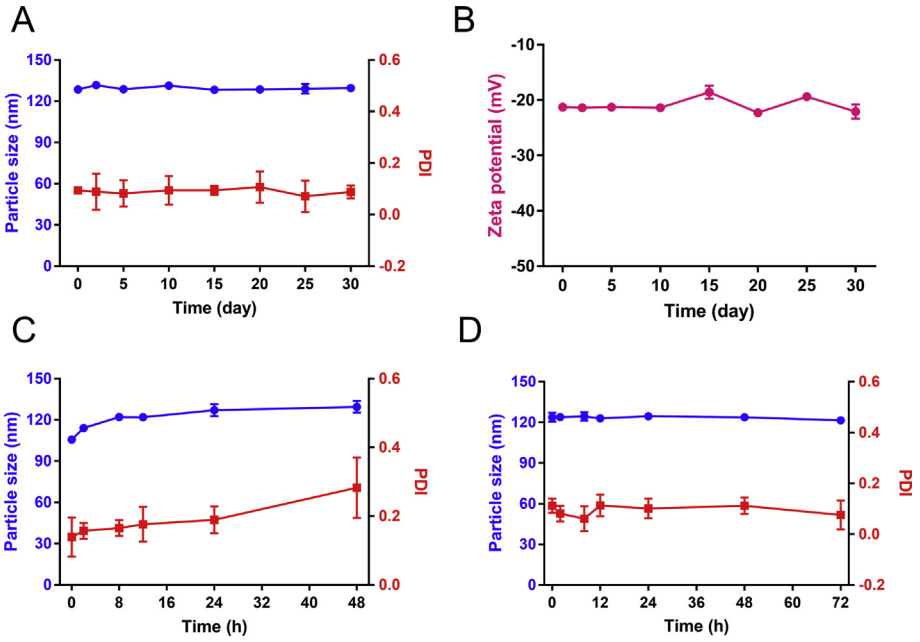


**Figure 3** (A) The particle size, PDI and (B) zeta potential variation of PSD LPs at 4 °C for 30 days, the particle size and PDI of PSD NPs (C) and PSD LPs (D) incubated in PBS containing 10% FBS (*v*/*v*) under 100 rpm shaking at 37 °C. Data were presented as mean ± SD ($n$ = 3).

compared to that of free PSD, indicating that the $Cu^{2+}$ is potentially capable of complexing with the compound PSD. What's more, the UV absorption spectrum of PSD LPs was similar to $Cu^{2+}$−PSD, which demonstrated the generation of $Cu^{2+}$−PSD in the inner aqueous phase of liposomes. On the other hand, the formation of $Cu^{2+}$−PSD complex inside liposomes was apparently observed with a color change from red to purple after drug loading (Fig. 2E), which was easily detected by eyes. Thus, all the data confirmed that the complex $Cu^{2+}$−PSD was successfully generated in the intraliposomal aqueous phase, and the compound PSD was loaded into the inner aqueous phase of liposomes rather than lipid bilayer. This would be attributed to the small amount of DMSO and $Cu^{2+}$. It was reported that the addition of DMSO could improve the solubility of the insoluble drug and enhance liposomal membrane permeability[18,28]. On the other hand, once the PSD was loaded into the intraliposomal aqueous phase, it would bind with $Cu^{2+}$ to form a water-insoluble complex $Cu^{2+}$−PSD, thus, in turn, would facilitate to the process of drug loading.

The TEM micrograph suggested that PSD LPs were nearly spherical and the particle size was in accordance with the results determined by dynamic light scattering (DLS, Fig. 2F).

### 3.3. *Physical stability of PSD NPs and PSD LPs*

As shown in Fig. 3, PSD LPs could be stored at 4 °C for at least 1 month with no obvious change in particle size, PDI and zeta potential. Besides, after incubating with PBS containing 10% FBS, PSD LPs displayed nearly the same particle size and PDI as previously for even 72 h. Nevertheless, PSD NPs exhibited an apparent increase in particle size and PDI. What's more, after incubated with PBS containing 10% FBS for 48 h, the solution for PSD NPs appeared obvious insoluble substance (data not shown). Therefore, PSD LPs displayed more excellent stability in comparison with PSD NPs.

### 3.4. *In vitro drug release*

There has been reported that the thioether linkage could be activated by ROS and GSH[29−32]. Thus, the *in vitro* drug release of PSD LPs was investigated under the condition of PBS (pH 7.4) containing 15% ethanol (*v*/*v*) and 10 mmol/L EDTA, with 10 mmol/L $H_2O_2$ or 10 mmol/L DTT or 0 mmol/L $H_2O_2$/DTT. As shown in Fig. 4, there was only a small amount of PTX and DOX (around 15%) were released from PSD LPs in the release medium containing 0 mmol/L $H_2O_2$/DTT within 24 h. However, in the presence of 10 mmol/L DTT or 10 mmol/L $H_2O_2$, the PSD LPs exhibited a faster release rate, especially for the oxidation condition with about 60% of PTX released within 24 h. Thus, the release of PSD LPs exhibited a redox dual-responsive property. On the other hand, according to the previous study, under the same condition, the PSD LPs demonstrated a slower release ratio by contrast to PSD NPs[16]. We speculated that this could be attributed to the stable lipid bilayer of liposomes and the formation of water-insoluble complexation $Cu^{2+}$−PSD.

### 3.5. *Cytotoxicity assay*

The MTT assay was utilized to evaluate *in vitro* cytotoxicity of blank Cu Glu LPs, PSD NPs and PSD LPs against breast cancer cells (4T1) and prostatic cancer cells (RM-1). The $IC_{50}$ values were calculated and summarized in Table 2. As shown in Fig. 5, the blank Cu Glu liposomes exhibited slight toxicity against 4T1 and RM-1 cells. We speculated that this could be ascribed to the generation of Fenton-like reactions catalyzed by $Cu^{2+}$ [33−35]. The $IC_{50}$ for PSD NPs and PSD LPs against 4T1 cells at 48 h was 65.49 and 175.3 nmol/L, for which was 147.9 and 372.2 nmol/L against RM-1 cells at 48 h, respectively. The results indicated that the preparations seemed more sensitive to 4T1 cells compared to RM-1 cells with a lower $IC_{50}$ value. We speculated that the preparations could generate a more potent anti-cancer effect in 4T1 tumor-bearing mice.

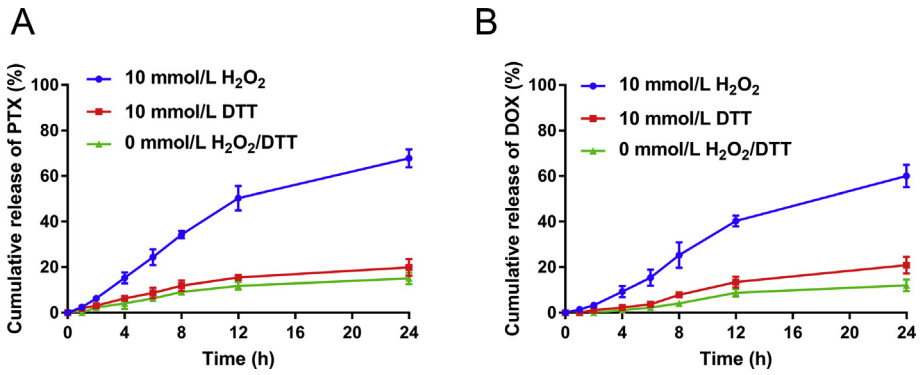


**Figure 4** Cumulative release of PTX (A) and DOX (B) from PSD LPs in PBS (pH 7.4), containing 15% ethanol (*v*/*v*) and 10 mmol/L EDTA, with 0 mmol/L $H_2O_2$/DTT or 10 mmol/L $H_2O_2$ or 10 mmol/L DTT. Data were presented as mean ± SD ($n$ = 3).

**Table 2** $IC_{50}$ values (nmol/L) of blank Cu Glu LPs, PSD NPs, and PSD LPs against 4T1 and RM-1 cells.

| Formulation | $IC_{50}$ (nmol/L) | | | |
|---|---|---|---|---|
| | 4T1 | | RM-1 | |
| | 48 h | 72 h | 48 h | 72 h |
| Blank Cu Glu LPs | – | – | – | – |
| PSD NPs | 65.49 ± 12.01 | 33.93 ± 5.06 | 147.9 ± 28.3 | 46.64 ± 4.88 |
| PSD LPs | 175.3 ± 17.76 | 72.97 ± 7.24 | 372.2 ± 60.11 | 80.64 ± 5.77 |

Data are mean ± SD, $n$ = 3.

The inhibition of preparations against 4T1 and RM-1 cells displayed a time- and concentration-dependent behavior, which was remarkably increased with the extension of time and enhancement of drug concentration (Fig. 5 and Supporting Information Fig. S2). In addition, PSD LPs exhibited slightly reduced cytotoxicity in comparison with PSD NPs. The reason could attribute to the following two aspects. On the one hand, PEGylation could hinder the cell uptake of particles in some

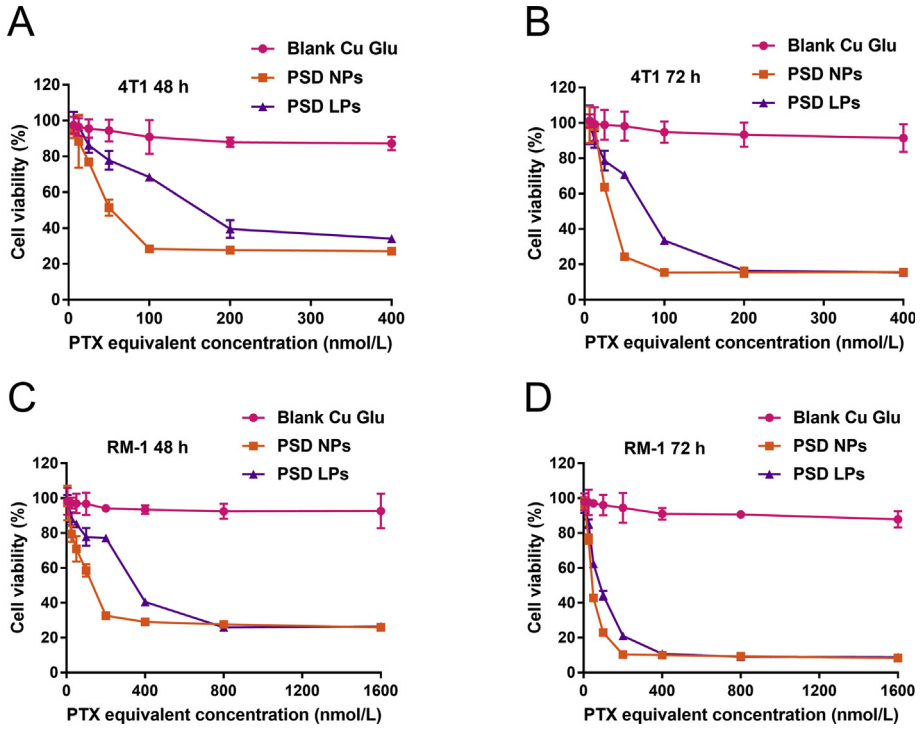


**Figure 5** Cell viability treated with various concentrations of blank Cu Glu liposomes, PSD NPs and PSD LPs against 4T1 cells for 48 h (A) and 72 h (B), against RM-1 cells for 48 h (C) and 72 h (D). Data were presented as mean ± SD ($n$ = 3).

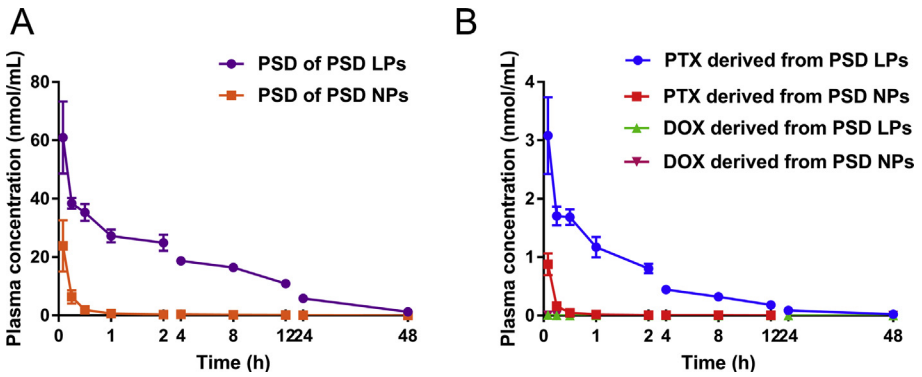


**Figure 6** Pharmacokinetic profiles of PSD NPs and PSD LPs. Molar concentration−time curves of (A) the prodrug PSD, (B) the released PTX and DOX. Data were presented as mean ± SD ($n = 3$).

degree. However, the PEG layer of nanoparticles was not as stable as that of liposomes. On the other hand, the drug release rate of preparations also influenced the *in vitro* cytotoxicity. Compared with the surface adsorption stabilizer of nanoparticles, the lipid bilayer of liposomes could effectively delay the release of drug. Thus, the PSD LPs demonstrated a lower *in vitro* cytotoxicity.

### 3.6. *Pharmacokinetic study*

Encouraged by the outstanding *in vitro* stability, the pharmacokinetic behavior of PSD NPs and PSD LPs was investigated and compared utilizing Sprague-Dawley rats. The plasma profiles of PSD NPs and PSD LPs were shown in Fig. 6. The results indicated that PSD NPs were rapidly eliminated from the plasma after intravenous administration, and remained little residual in blood after 1 h, which could be ascribed to the instability of PSD NPs in blood. Nevertheless, the PSD LPs displayed an enhanced plasma concentration at any determined time and a decreased elimination rate by contrast to PSD NPs, which manifested an excellently prolonged circulation in plasma.

The pharmacokinetic parameters were acquired by fitting the plasma profile with non-compartmental model and were summarized in Supporting Information Table S1. The area under the curve (AUC) of PSD LPs for prodrug PSD was 418.38 ± 42.61 nmol/mL h, which were enhanced 32.9 times in comparison with PSD NPs. What's more, PSD LPs also exhibited 1.3-fold prolonged half-time, 1.6-fold extended mean residence time (MRT) and 35-fold decreased clearance relative to PSD NPs. However, to our surprise, the concentration of released DOX was significantly lower than that of PTX. We hypothesized that the released DOX from PSD could mainly exist in other forms of fragments containing DOX, due to the difficulty of amido bond to hydrolyze[36]. In short, the results indicated that the PSD LPs exhibited remarkably prolonged systemic circulation time compared with PSD NPs, which could be beneficial to the accumulation of PSD LPs at the tumor site.

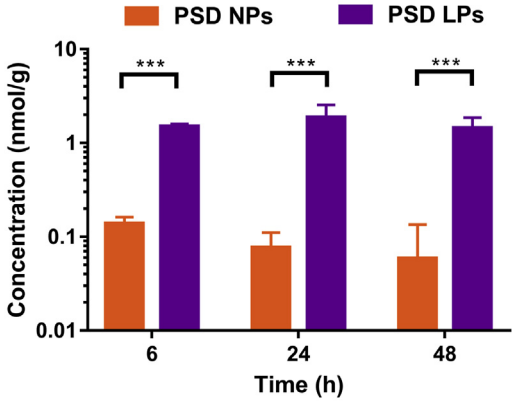


**Figure 7** Direct quantitation of PSD NPs and PSD LPs in tumors for 6, 24 and 48 h post-injection. Data were presented as mean ± SD ($n = 3$). $^{***}P < 0.001$.

### 3.7. *In vivo bio-distribution study*

With the significantly extended blood circulation, the *in vivo* bio-distribution of PSD NPs and PSD LPs was investigated in 4T1 tumor-bearing BALB/c mice. DiR-labeled PSD NPs and DiR-labeled PSD LPs were intravenously administrated *via* the tail vein. *In vivo* fluorescence signal was continuously monitored until 48 h using an IVIS. As shown in Supporting Information Fig. S3A, the fluorescence intensity at the tumor site was gradually increased with the time extended for both DiR-labeled PSD NPs and PSD LPs until 24 h when the tumor accumulation reached peaking. However, there was an obviously decreased fluorescence signal observed at tumor treated with DiR-labeled PSD NPs at 48 h. On the other hand, the mice treated with DiR-labeled PSD LPs demonstrated a comparative fluorescence intensity with 24 h. In addition, the tumors and major organs were harvested at 24 or 48 h post-injection for *ex vivo* fluorescence imaging, and the semiquantitative fluorescence intensity of *ex vivo* bio-distribution was shown in Fig. S3B−S3E. The results were consistent with *in vivo* fluorescence imaging.

The direct quantitation of PSD NPs and PSD LPs in tumors was determined using a microplate reader. As shown in Fig. 7, at any determined point, the drug's concentration of PSD LPs was more than 10 times higher than that of PSD NPs in tumors. Furthermore, the distribution of PSD LPs at the tumor site was nearly close to each other from 6 to 48 h and reached the peak at 24 h. The result was consistent with the *in vivo* pharmacokinetic behavior. Thus, all the results demonstrated the PSD LPs exhibited higher tumor accumulation compared with PSD NPs. This would be attributed to the prolonged blood circulation, which in turn would benefit the tumor accumulation *via* the EPR effect.

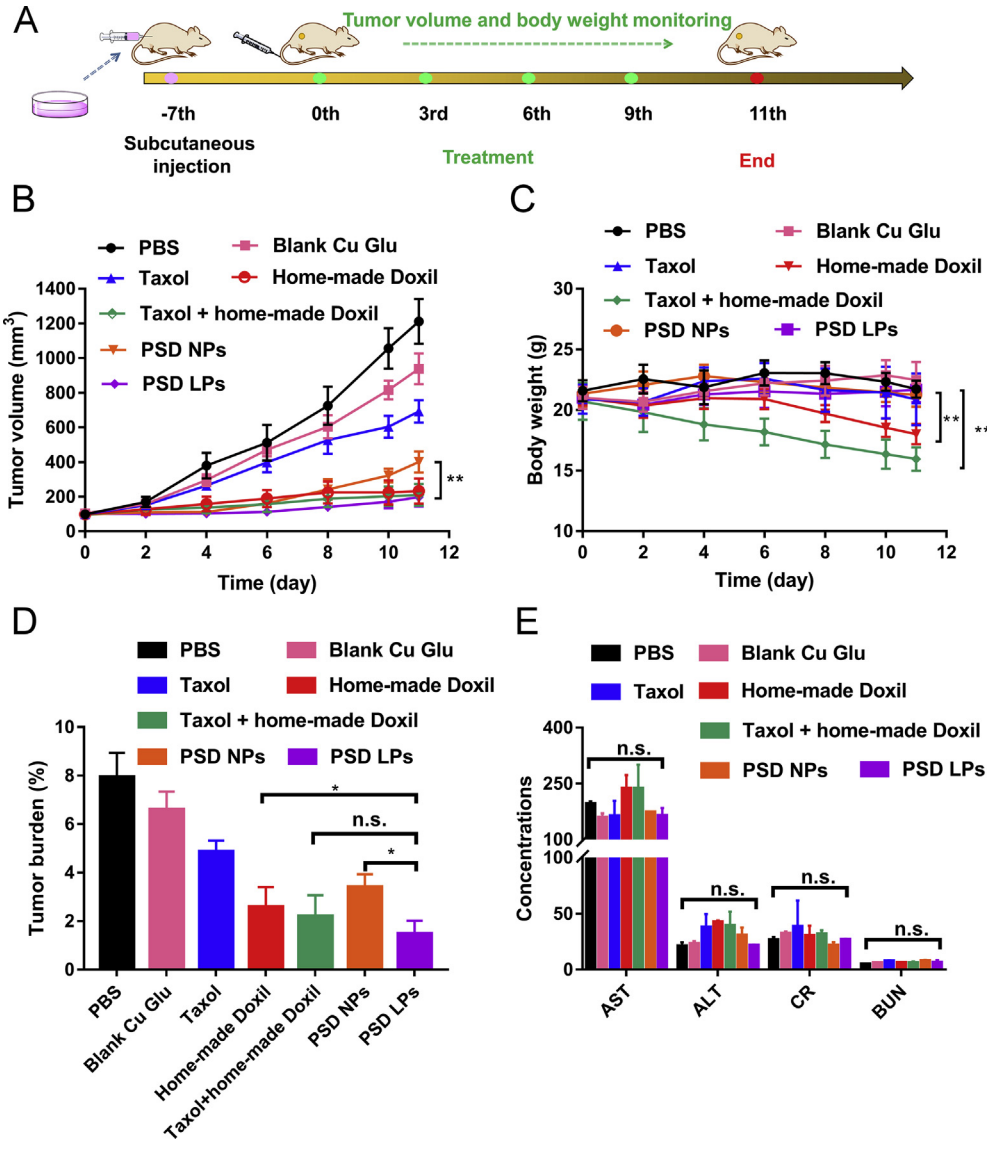


**Figure 8** *In vivo* antitumor effect of PSD LPs. (A) Therapeutic schedule for PSD LPs mediated combination therapy. (B) Tumor growth curves and (C) body weight change curves post-injection of different formulations ($n = 5$). (D) Tumor burden rate ($n = 5$) and (E) hematological biochemical parameters of different formulations after treatment (the unit for AST, ALT, BUN, and CR is U/L, U/L, mmol/L, and μmol/L, respectively, $n = 3$). Data were presented as mean ± S.D. $^{*}P < 0.05$, $^{**}P < 0.01$, $^{***}P < 0.001$.

### 3.8. *In vivo anticancer efficacy study*

Encouraged by the promising effect *in vitro* cytotoxicity, outstanding systemic circulation and tumor accumulation, the antitumor activity of PSD NPs and PSD LPs was investigated in a 4T1 xenograft tumor model. When the tumor volume reached approximately 100 $mm^3$, the mice were randomly divided into seven groups and treated with saline, blank Cu Glu LPs, Taxol, Doxil, Taxol + Doxil, PSD NPs and PSD LPs *via* tail vein, respectively. As shown in Fig. 8B, there was a rapid increase in tumor volume for saline group. The PSD NPs group exhibited a certain degree of suppression of tumor growth. However, the inhibition ratio of tumor growth for PSD LPs group was significantly superior to that of PSD NPs ($P < 0.01$). This should be ascribed to the prolonged blood circulation and improved tumor accumulation of PSD LPs. In addition, a home-made Doxil and a physical mixture of Taxol and Doxil were also utilized as a comparison. During the experiment, the Taxol + Doxil mixture group displayed nearly the same inhibition of tumor growth compared with PSD LPs.

However, the body weight of home-made Doxil and Taxol + Doxil groups was remarkably decreased post-injection. And the H&E staining histological images showed that there was an obvious hemorrhage and drug residue in spleen for Doxil and Taxol + Doxil groups (Supporting Information Fig. S4). Thus, we speculated that the serious loss of body weight could result from the superfluous accumulation of DOX at normal tissues, which indicated toxicity. Furthermore, Doxil and Taxol + Doxil groups also demonstrated myocardial fiber rupture (as the black arrows pointed in Fig. S4), indicating cardiotoxicity. By contrast, the PSD LPs displayed no obvious loss of body weight and damage of normal tissue, demonstrating better biocompatibility and the potential to improve the maximum tolerated dose (MTD) for a more potent anti-tumor effect (Fig. 8C). What's more, the hepatic and

renal function of mice has confirmed no obvious differentiation by measuring the aspartate transaminase (AST), alanine transaminase (ALT), blood urea nitrogen (BUN) and creatinine (CR) in the blood of mice (Fig. 8E). In a nutshell, the results suggested that PSD LPs displayed a more significant anti-tumor efficacy compared to PSD NPs and good biocompatibility as a safe formulation.

## 4. Conclusions

In this study, we successfully encapsulated the heterodimeric prodrug PSD synthesized previously into the intraliposomal aqueous phase of liposomes utilizing a copper ion gradient. The prepared liposomes displayed a high encapsulation efficacy (nearly 100%) and loading capacity (>15%). The prodrug PSD could respond to the stimulation of tumor microenvironment with high ROS/GSH to release parent drugs. Furthermore, the stimuli-responsive PSD LPs were demonstrated with excellent storage stability, prolonged blood circulation, improved accumulation at the tumor site, and more efficient suppression of tumor growth in comparison with PSD NPs. Moreover, the PSD LPs exhibited lower cardiotoxicity and kidney damage compared with the Taxol and Doxil mixture at equivalent dosage, demonstrating better biocompatibility and the potential to improve the maximum tolerated dose (MTD). Thus, the PSD LPs were proved to be a more efficient formulation. On the other hand, this technology provided a novel pathway to co-deliver doxorubicin and other hydrophobic chemotherapeutic drugs for combination therapy with high efficacy and low toxicity.

## Acknowledgments

This research was supported by National Science and Technology Major Projects for Major New Drugs Innovation and Development (No. 2017ZX09101-001-005, Beijing, China), Science and Technology Plan Project of Shenyang (No. 18-400-4-08, Z17-5-064, China) and the Career Development Program for Young and Middle-aged Teachers in Shenyang Pharmaceutical University (Shenyang, China).

## Author contributions

Yu Jiang: investigation, original draft writing, visualization, formal analysis, and data curation. Wang Yingli: conceptualization, methodology, writing review and editing. Zhou Shuang: investigation, writing review and editing. Li Jinbo: investigation and validation. Wang Jiamei: investigation. Chi Dongxu: visualization and software. Wang Xue: investigation. Lin Guimei: writing review and editing. He Zhonggui: resources. Wang Yongjun: conceptualization, methodology, writing review and editing, supervision, project administration, and funding acquisition.

## Conflicts of interest

The authors declare no conflicts of interest.

## Appendix A. Supporting information

Supporting data to this article can be found online at https://doi.org/10.1016/j.apsb.2020.04.011.

## References

1. Gerber HP, Ferrara N. Pharmacology and pharmacodynamics of bevacizumab as monotherapy or in combination with cytotoxic therapy in preclinical studies. *Cancer Res* 2005;**65**:671−80.
2. Hu Q, Sun W, Wang C, Gu Z. Recent advances of cocktail chemotherapy by combination drug delivery systems. *Adv Drug Deliv Rev* 2016;**98**:19−34.
3. Zhang R, Zhang Y, Zhang Y, Wang X, Gao X, Liu Y, et al. Ratiometric delivery of doxorubicin and berberine by liposome enables superior therapeutic index than Doxil®. *Asian J Pharm Sci* 2019. https://doi.org/10.1016/j.ajps.2019.04.007.
4. Na K, Liu K, Yu J, Wang X, Li M, Tian C, et al. A solvent-assisted active loading technology to prepare gambogic acid and all-trans retinoic acid co-encapsulated liposomes for synergistic anticancer therapy. *Drug Deliv Transl Res* 2019;**10**:146−58.
5. Feng C, Zhang H, Chen J, Wang S, Xin Y, Qu Y, et al. Ratiometric co-encapsulation and co-delivery of doxorubicin and paclitaxel by tumor-targeted lipodisks for combination therapy of breast cancer. *Int J Pharm* 2019;**560**:191−204.
6. Wang H, Zhao Y, Wu Y, Hu YL, Nan K, Nie G, et al. Enhanced anti-tumor efficacy by co-delivery of doxorubicin and paclitaxel with amphiphilic methoxy PEG−PLGA copolymer nanoparticles. *Biomaterials* 2011;**32**:8281−90.
7. Yuan M, Qiu Y, Zhang L, Gao H, He Q. Targeted delivery of transferrin and TAT co-modified liposomes encapsulating both paclitaxel and doxorubicin for melanoma. *Drug Deliv* 2016;**23**:1171−83.
8. Skwarczynski M, Hayashi Y, Kiso Y. Paclitaxel prodrugs: toward smarter delivery of anticancer agents. *J Med Chem* 2006;**49**:7253−69.
9. Tishler RB, Geard CR, Hall EJ, Schiff PB. Taxol sensitizes human astrocytoma cells to radiation. *Cancer Res* 1992;**52**:3495−7.
10. Sun D, Ding J, Xiao C, Chen J, Zhuang X, Chen X. Preclinical evaluation of antitumor activity of acid-sensitive PEGylated doxorubicin. *ACS Appl Mater Interfaces* 2014;**6**:21202−14.
11. Liu Y, Fang J, Kim YJ, Wong MK, Wang P. Codelivery of doxorubicin and paclitaxel by cross-linked multilamellar liposome enables synergistic antitumor activity. *Mol Pharm* 2014;**11**:1651−61.
12. Shim G, Kim MG, Kim D, Park JY, Oh YK. Nanoformulation-based sequential combination cancer therapy. *Adv Drug Deliv Rev* 2017;**115**:57−81.
13. Jia J, Zhu F, Ma X, Cao ZW, Li YX, Chen YZ. Mechanisms of drug combinations: interaction and network perspectives. *Nat Rev Drug Discov* 2009;**8**:111−28.
14. Duska LR, Penson R, Supko JG, Finkelstein DM, Makastorsis T, Gallagher J, et al. A phase I study of continuous infusion doxorubicin and paclitaxel chemotherapy with granulocyte colony-stimulating factor for relapsed epithelial ovarian cancer. *Clin Cancer Res* 1999;**5**:1299−305.
15. Markovsky E, Baabur-Cohen H, Satchi-Fainaro R. Anticancer polymeric nanomedicine bearing synergistic drug combination is superior to a mixture of individually-conjugated drugs. *J Control Release* 2014;**187**:145−57.
16. Wang Y, Wang J, Yang L, Wei W, Sun B, Na K, et al. Redox dual-responsive paclitaxel−doxorubicin heterodimeric prodrug self-delivery nanoaggregates for more effective breast cancer synergistic combination chemotherapy. *Nanomedicine* 2019;**21**:102066.
17. Dawidczyk CM, Kim C, Park JH, Russell LM, Lee KH, Pomper MG, et al. State-of-the-art in design rules for drug delivery platforms: lessons learned from FDA-approved nanomedicines. *J Control Release* 2014;**187**:133−44.
18. Tang WL, Tang WH, Szeitz A, Kulkarni J, Cullis P, Li SD. Systemic study of solvent-assisted active loading of gambogic acid into liposomes and its formulation optimization for improved delivery. *Biomaterials* 2018;**166**:13−26.
19. Liu J, Chi D, Pan S, Zhao L, Wang X, Wang D, et al. Effective co-encapsulation of doxorubicin and irinotecan for synergistic therapy using liposomes prepared with triethylammonium sucrose octasulfate as drug trapping agent. *Int J Pharm* 2019;**557**:264−72.

20. Bernabeu E, Cagel M, Lagomarsino E, Moretton M, Chiappetta DA. Paclitaxel: what has been done and the challenges remain ahead. *Int J Pharm* 2017;**526**:474−95.
21. Zhang JA, Anyarambhatla G, Ma L, Ugwu S, Xuan T, Sardone T, et al. Development and characterization of a novel Cremophor® EL free liposome-based paclitaxel (LEP−ETU) formulation. *Eur J Pharm Biopharm* 2005;**59**:177−87.
22. Kheirolomoom A, Mahakian LM, Lai CY, Lindfors HA, Seo JW, Paoli EE, et al. Copper−doxorubicin as a nanoparticle cargo retains efficacy with minimal toxicity. *Mol Pharm* 2010;**7**:1948−58.
23. Lei M, Ma M, Pang X, Tan F, Li N. A dual pH/thermal responsive nanocarrier for combined chemo-thermotherapy based on a copper−doxorubicin complex and gold nanorods. *Nanoscale* 2015;**7**:15999−6011.
24. Kheirolomoom A, Lai C-Y, Tam SM, Mahakian LM, Ingham ES, Watson KD, et al. Complete regression of local cancer using temperature-sensitive liposomes combined with ultrasound-mediated hyperthermia. *J Control Release* 2013;**172**:266−73.
25. Wallace KB. Nonenzymatic oxygen activation and stimulation of lipid peroxidation by doxorubicin−copper. *Toxicol Appl Pharmacol* 1986;**86**:69−79.
26. May P, Williams G, Williams D. Solution chemistry studies of adriamycin−iron complexes present *in vivo*. *Eur J Cancer* 1980;**16**:1275−6.
27. Triton T, Yee G. The anticancer agent adriamycin can be actively cytotoxic without entering cells. *Science* 1982;**217**:248−50.
28. Pauli G, Tang WL, Li SD. Development and characterization of the solvent-assisted active loading technology (SALT) for liposomal loading of poorly water-soluble compounds. *Pharmaceutics* 2019;**11**:465.
29. Li M, Zhao L, Zhang T, Shu Y, He Z, Ma Y, et al. Redox-sensitive prodrug nanoassemblies based on linoleic acid-modified docetaxel to resist breast cancers. *Acta Pharm Sin B* 2019;**9**:421−32.
30. Wang K, Yang B, Ye H, Zhang X, Song H, Wang X, et al. Self-strengthened oxidation-responsive bioactivating prodrug nanosystem with sequential and synergistically facilitated drug release for treatment of breast cancer. *ACS Appl Mater Interfaces* 2019;**11**:18914−22.
31. Luo C, Sun J, Liu D, Sun B, Miao L, Musetti S, et al. Self-assembled redox dual-responsive prodrug-nanosystem formed by single thioether-bridged paclitaxel-fatty acid conjugate for cancer chemotherapy. *Nano Lett* 2016;**16**:5401−8.
32. Sun B, Luo C, Zhang X, Guo M, Sun M, Yu H, et al. Probing the impact of sulfur/selenium/carbon linkages on prodrug nanoassemblies for cancer therapy. *Nat Commun* 2019;**10**:3211.
33. Reybier K, Ayala S, Alies B, Rodrigues JV, Bustos Rodriguez S, La Penna G, et al. Free superoxide is an intermediate in the production of $H_2O_2$ by copper (I)-A$\beta$ peptide and $O_2$. *Angew Chem Int Ed* 2016;**55**:1085−9.
34. Lin LS, Huang T, Song J, Ou XY, Wang Z, Deng H, et al. Synthesis of copper peroxide nanodots for $H_2O_2$ self-supplying chemodynamic therapy. *J Am Chem Soc* 2019;**141**:9937−45.
35. Ma B, Wang S, Liu F, Zhang S, Duan J, Li Z, et al. Self-assembled copper−amino acid nanoparticles for *in situ* glutathione "AND" $H_2O_2$ sequentially triggered chemodynamic therapy. *J Am Chem Soc* 2018;**141**:849−57.
36. Zhou F, Feng B, Wang T, Wang D, Cui Z, Wang S, et al. Theranostic prodrug vesicles for reactive oxygen species-triggered ultrafast drug release and local-regional therapy of metastatic triple-negative breast cancer. *Adv Funct Mater* 2017;**27**:1703674.